# Comparison of GLR and Invariant Detectors under Structured Clutter Covariance

Hyung Soo Kim and Alfred O. Hero, III, *Fellow, IEEE*

Department of Electrical Engineering and Computer Science
University of Michigan
1301 Beal Avenue
Ann Arbor, MI 48109-2122
Tel: (734) 763-0564
Fax: (734) 763-8041
Email: {kimhs,hero}@eecs.umich.edu

**Abstract**

This paper addresses a target detection problem in radar imaging for which the covariance matrix of unknown Gaussian clutter has block diagonal structure. This block diagonal structure is the consequence of a target lying along a boundary between two statistically independent clutter regions. Here we design adaptive detection algorithms using both the generalized likelihood ratio (GLR) and the invariance principles. There has been considerable recent interest in applying invariant hypothesis testing as an alternative to the GLR test. This interest has been motivated by several attractive properties of invariant tests including: exact robustness to variation of nuisance parameters and possible finite-sample min-max optimality. However, in our deep-hide target detection problem, there are regimes for which neither the GLR nor the invariant tests uniformly outperforms the other. We will discuss the relative advantages of GLR and invariance procedures in the context of this radar imaging and target detection application.

This work was supported in part by the Air Force Office of Scientific Research under MURI grant: F49620-97-0028. Part of this work appeared in "Adaptive target detection across a clutter boundary: GLR and maximally invariant detectors," in *Proc. IEEE Intl. Conf. Image Processing*, Vancouver, Canada, Sep. 2000.

The authors are with the Department of Electrical Engineering and Computer Science, University of Michigan, Ann Arbor, MI 48109-2122 (Email: {kimhs,hero}@eecs.umich.edu).

## I. Introduction

In this paper adaptive detection algorithms are developed for imaging radar targets in *structured* clutter by exploiting both the generalized likelihood ratio (GLR) principle and the invariance principle. In automatic target recognition, it is important to be able to reliably detect or classify a target in a manner which is robust to target and clutter variability yet maintains the highest possible discrimination capability. The GLR and invariance principles are worthwhile approaches since they often yield good constant false alarm rate (CFAR) tests. The GLR principle implements the intuitive estimate-and-plug principle: replacing all unknowns in the likelihood ratio (LR) test by their maximum likelihood estimates (MLEs). In contrast, application of the invariance principle seeks to project away the clutter parameters by compressing the observations down to a lower-dimensional statistic while retaining the maximal amount of information for discrimination of the target [1], [2], [3], [4]. This statistic is called the maximal invariant and, if one is lucky, the form of the most powerful LR test based on the maximal invariant does not depend on the nuisance parameters, resulting in a uniformly most powerful (UMP) invariant test [5], [6]. Despite the difficulty in finding maximal invariants and their statistical distributions, the payoff for the extra effort in signal processing applications can be high [5], [6], [7]. We will demonstrate such a payoff for a radar detection problem.

A common assumption in homogeneous but uncertain clutter scenarios is that the target is of known form but unknown amplitude in Gaussian noise whose covariance matrix is totally unknown or *unstructured*. This assumption induces parameter uncertainty for which the general multivariate analysis of variance (GMANOVA) model applies and optimal and suboptimal detection algorithms can be easily derived using the GLR principle [8], [9], [10], [11]. Different adaptive detectors were derived in [12] and [13] for the case of optical images. However, when some structure on the covariance matrix is known *a priori*, improvements over this GLR test are possible, e.g. [14]. Bose and Steinhardt [7] proposed an invariant detector which outperforms the GLR [9] for unstructured covariance when the noise covariance matrix is assumed to have *a priori* known block diagonal structure. In [15], the difficult deep-hide scenario was considered where the target parks along a known boundary separating two adjacent clutter regions, e.g. an agricultural field and a forest canopy. It was shown there that under the reasonable assumption that the two clutter types are statistically independent, the induced block diagonal covariance structure can be used to derive an invariant test with performance advantage similar to Bose

and Steinhardt's test.

In this paper we derive the form of the GLR for block structured covariance. Then the invariant approach considered in [7] and [15] is developed in the context of imaging radar for deep-hide targets and compared to the GLR. In this context the spatial component has clutter covariance matrix $\mathbf{R}$ which decomposes into a block diagonal matrix under an independence assumption between the two clutter regions. Several cases, denoted in decreasing order of uncertainty as Cases 1, 2 and 3, of block diagonal covariance matrices are examined:

$$\mathbf{R} = \begin{bmatrix} \mathbf{R}_A & \mathbf{O} \\ \mathbf{O} & \mathbf{R}_B \end{bmatrix} \tag{1}$$

- Case 1: $\mathbf{R}_A > 0$, $\mathbf{R}_B > 0$
- Case 2: $\mathbf{R}_A > 0$, $\mathbf{R}_B = \sigma^2 \mathbf{I}$ where $\sigma^2 > 0$
- Case 3: $\mathbf{R}_A > 0$, $\mathbf{R}_B = \mathbf{I}$

where the subscripts denote the two different regions A and B. Case 1 corresponds to two completely unknown clutter covariance matrices $\mathbf{R}_A$ and $\mathbf{R}_B$, and Case 2 corresponds to one clutter covariance $\mathbf{R}_A$ completely unknown and the other $\mathbf{R}_B$ known up to a scale parameter. As shown in [7] the known clutter covariance matrix in $\mathbf{R}_B$, represented by the matrix $\mathbf{I}$, can be taken as the identity matrix without loss of generality. Case 3 corresponds to $\mathbf{R}_B$ known exactly. Cases 2 and 3 arise, for example, in application where one of the clutter regions is well characterized. The maximal invariant statistics for Cases 1 and 2 were previously derived by Bose and Steinhardt in [7] and invariant tests were also proposed based on these statistics. We treat Cases 1-3 in a unified framework and propose alternative maximal invariant (MI) tests which are better adapted to the deep-hide target application. We show via simulation that there are regimes of operation which separate the performance of the GLR and MI tests. When there are a large number of independent snapshots of the clutter, the MLEs of the target amplitude and the block diagonal clutter covariance are reliable and accurate, and the GLR test performs as well as the MI test. Conversely, when a limited number of snapshots are available and SNR is low, the MLEs are unreliable and the MI test outperforms the GLR test. This property is also confirmed by the real data example, i.e. the MI test can detect weaker targets than the other tests when the number of snapshots is few.

In Section II the image model for the detection problem is introduced and a canonical form is obtained by coordinate transformation. We then review the principles of GLR and invariance

in Section III. Kelly's GLR test [9] for an unstructured covariance matrix is derived as an illustration of these two principles. Section IV then reviews the application of these principles to detect a target across a clutter boundary. We also extend the detection problem from a single target to one of multiple targets in Section V. Finally, the relational performances between the GLR and MI tests are explored by analysis and by simulation. Due to space limitations most of the mathematical derivations have been omitted from this paper. These can be found in [16].

## II. Image Model

Let $\{\underline{x}_i\}_{i=1}^n$ be $n$ statistically independent $m \times 1$ complex Gaussian vectors constructed by raster scanning a set of $n$ 2-D images (snapshots). We call each of these vectors subimages or chips and assume that they each have identical $m \times m$ covariance matrices $\mathbf{R}$ but with possibly different mean vectors (targets). Then the measurement image matrix $(m \times n)$ $\mathbf{X} = [\underline{x}_1, \ldots, \underline{x}_n]$ can be modeled as follows

$$\mathbf{X} = \mathbf{S}\,\underline{a}\,\underline{b}^H + \mathbf{N} \tag{2}$$

where $\mathbf{S} = [\underline{s}_1, \ldots, \underline{s}_p]$ is an $m \times p$ matrix consisting of signature vectors of $p$ possible targets, $\underline{a} = [a_1, \ldots, a_p]^T$ is a $p \times 1$ unknown target amplitude vector for $p$ targets, and $\underline{b}^H = [b_1, \ldots, b_n]$ is a $1 \times n$ target location vector which accounts for the presence of targets in each subimage. While this model allows multiple target signatures to exist simultaneously in a chip, we concentrate here on the case that $\underline{a}$ has only one non-zero element, i.e. at most one of a possible $p$ signatures can be present. This model (2) implies that the target components in different subimages differ only by a scale factor. Also $\mathbf{N}$ is a complex multivariate Gaussian matrix with i.i.d. columns: $vec(\mathbf{N}) \sim \mathcal{CN}(\underline{0}, \mathbf{R} \bigotimes \mathbf{I}_n)$ where $\underline{0}$ is an $mn \times 1$ zero vector, $\mathbf{I}_n$ is an $n \times n$ identity matrix, and $\bigotimes$ is the Kronecker product. It is common to model a complex valued radar image as linear in the target with additive Gaussian distributed clutter. Examples where a Gaussian model is justified for terrain clutter can be found in [17]. Even in cases when such a model is not applicable to the raw data, a whitening and local averaging technique can be implemented to obtain a Gaussian approximation [13].

The detection problem is to seek the presence of target(s) for $\mathbf{S}$ and $\underline{b}$ known, $\underline{a}$ unknown, and the independent columns of $\mathbf{N}$ having the unknown covariance matrix $\mathbf{R}$. By applying coordinate rotations to both of the column space and the row space of $\mathbf{X}$ we can put the image model into

a convenient canonical form as in [18]. Let $\mathbf{S}$ and $\underline{b}$ have the QR decompositions

$$\mathbf{S} = \mathbf{Q}_S \begin{bmatrix} \mathbf{T}_S \\ \mathbf{O} \end{bmatrix}, \ \underline{b} = \mathbf{Q}_b \begin{bmatrix} t_b \\ \underline{0} \end{bmatrix}$$

where $\mathbf{Q}_S(m \times m)$, $\mathbf{Q}_b(n \times n)$ are unitary matrices, $\mathbf{T}_S$ is a $p \times p$ upper-triangular matrix, and $t_b$ is a scalar. Multiplying $\mathbf{X}$ on the left and right by $\mathbf{Q}_S^H$ and $\mathbf{Q}_b$, respectively, we have the canonical representation

$$\tilde{\mathbf{X}} = \begin{bmatrix} \mathbf{T}_S \\ \mathbf{O} \end{bmatrix} \underline{a} \left[ t_b^H \ \underline{0}^H \right] + \tilde{\mathbf{N}}$$

where $\tilde{\mathbf{N}}$ is still $n$-variate normal with zero mean and $cov[vec(\tilde{\mathbf{N}})] = \mathbf{Q}_S^H \mathbf{R} \mathbf{Q}_S \bigotimes \mathbf{I}_n$, and the target detection problem is not altered since $\mathbf{R}$ is unknown. Now the transformed data has the partition

$$\tilde{\mathbf{X}} = \begin{bmatrix} \underline{x}_{11} & \mathbf{X}_{12} \\ \underline{x}_{21} & \mathbf{X}_{22} \end{bmatrix} \tag{3}$$

where $\underline{x}_{11}$ is a $p \times 1$ vector, $\underline{x}_{21}$ is a $(m-p) \times 1$ vector, $\mathbf{X}_{12}$ is $p \times (n-1)$, and $\mathbf{X}_{22}$ is $(m-p) \times (n-1)$. Note that $\mathbf{Q}_S^H$ and $\mathbf{Q}_b$ have put all the target energy into the first $p$ pixels of the first subimage, $\underline{x}_{11}$. In the sequel, unless stated otherwise, we will assume that the model has been put into this canonical form.

For the special case of $p = 1$ (single target), this model reduces to the one studied by Kelly [9]

$$\mathbf{X} = a \, \underline{\varepsilon}_1 \, \underline{e}_1^T + \mathbf{N} \tag{4}$$

where $a$ is an unknown complex amplitude, $\underline{e}_1 = [1, 0, \ldots, 0]^T$ is the $n \times 1$ unit vector, and the known target signature is transformed into an $m \times 1$ unit vector $\underline{\varepsilon}_1$. In this case, the first column of $\mathbf{X}$ will be called primary data while the rest will be called secondary data. With the model (4) we can denote the unknowns by the unknown parameter vector $\theta = \{a, \mathbf{R}\} \in \Theta$ where $\Theta$ is the prior parameter range of uncertainty. Let $\Theta_0$ and $\Theta_1$ partition the parameter space into target absent ($H_0$) and target present ($H_1$) scenarios: $\Theta_0 = \{a, \mathbf{R} : a = 0, \mathbf{R} \in \text{Hermitian}(m \times m)\}$, $\Theta_1 = \{a, \mathbf{R} : a \neq 0, \mathbf{R} \in \text{Hermitian}(m \times m)\}$. Then the general form for the detection problem is expressed via the two mutually exclusive hypotheses:

$$\begin{aligned} H_0 &: \ \mathbf{X} \sim f(\mathbf{X}; \theta_0), \ \theta_0 = \{0, \mathbf{R}\} \in \Theta_0 \\ H_1 &: \ \mathbf{X} \sim f(\mathbf{X}; \theta_1), \ \theta_1 = \{a, \mathbf{R}\} \in \Theta_1. \end{aligned}$$

Now, following [7], we extend (4) to the structured covariance case. Consider Case 1 in Section I. Then the target signature $\underline{s}$ is partitioned as $\underline{s} = [\underline{s}_A^H \ \underline{s}_B^H]^H$ where $\underline{s}_A$ and $\underline{s}_B$ are $m_A \times 1$ and $m_B \times 1$ column vectors, respectively ($m_A + m_B = m$). The unitary matrices $\mathbf{Q}_{S_A}$ and $\mathbf{Q}_{S_B}$ can be obtained from the QR decompositions of $\underline{s}_A$ and $\underline{s}_B$, respectively. Then using

$$\mathbf{Q}_S = \begin{bmatrix} \mathbf{Q}_{S_A} & \mathbf{O} \\ \mathbf{O} & \mathbf{Q}_{S_B} \end{bmatrix}$$

in the canonical transformation,the model is composed of two parts from regions A and B

$$\mathbf{X} = \begin{bmatrix} \mathbf{X}_A \\ \mathbf{X}_B \end{bmatrix} = a \begin{bmatrix} \underline{\tilde{s}}_A \\ \underline{\tilde{s}}_B \end{bmatrix} \underline{e}_1^T + \begin{bmatrix} \mathbf{N}_A \\ \mathbf{N}_B \end{bmatrix} \tag{5}$$

where $\underline{\tilde{s}}_A = [s_A, 0, \ldots, 0]^T$ and $\underline{\tilde{s}}_B = [s_B, 0, \ldots, 0]^T$. $\mathbf{N}_A$ $(m_A \times n)$ and $\mathbf{N}_B$ $(m_B \times n)$ are independent Gaussian matrices with unknown covariance matrices $\mathbf{R}_A$ $(m_A \times m_A)$ and $\mathbf{R}_B$ $(m_B \times m_B)$, respectively. The target detection problem is now simply stated as testing $a = 0$ vs. $a \neq 0$ in (5).

## III. Detection Theory

The aforementioned target detection problem is an example of testing composite hypotheses, i.e. there exist unknown "nuisance parameters" (clutter covariance and target amplitude) under both the null (target-absent) and alternative (target-present) hypotheses. This implies that the false alarm (FA) and detection probabilities of any detector will generally vary as a function of these unknowns. More importantly, only rarely is there a detector that is most powerful (MP) irrespective of these parameters, i.e. there exists no uniformly most powerful (UMP) test of any FA level.

UMP tests do not exist for the detection problem treated here. A popular alternative, but sub-optimal, strategy is to use the generalized likelihood ratio (GLR) principle. The GLR test is asymptotically UMP since, under broad conditions [19], MLEs are consistent estimators as the number of observations goes to infinity. Furthermore in many physical problems of interest, a GLR test will give satisfactory results [20]. In some instances, however, the optimization or maximization involved in deriving a GLR test may be intractable to obtain in closed form. Moreover, similarly to small sample MLEs, the performance of a GLR test can be poor (not even unbiased) in the finite sample regime [21]. In this section we review the principle of invariance

as an alternative strategy and apply to the case of unstructured clutter as an illustration. For a more detailed discussion with examples, refer to [22].

### A. Invariance Principle

The main idea behind the invariance principle is to find a statistic called the maximal invariant, which maximally condenses the data while retaining the model discrimination capability of the original data set. As contrasted with the minimax sufficient statistic [21], which maximally condenses the data while retaining the full parametric estimation capability of the original data, the maximal invariant preserves only the information necessary to detect the target as opposed to estimating its amplitude. More details on the relationship between sufficiency and maximal invariance are provided in [22]. Maximal invariants can be found when the probability model has functional invariance which can be characterized by group actions on the measurement space $\mathbf{X}$ and induced group actions on the parameter space $\Theta$. Let $\mathcal{G}$ be a group of transformations $g : \chi \to \chi$ acting on $\mathbf{X}$. Assume that for each $\theta \in \Theta$ there exists a unique $\bar{\theta} = \bar{g}(\theta)$ such that $f_\theta(g(\mathbf{X})) = f_{\bar{\theta}}(\mathbf{X})$. $\bar{g} \in \bar{\mathcal{G}}$ is called the induced group action on $\Theta$. The above relation implies that the natural invariance which exists in the parameter space of $\theta$ implies a natural invariance in the space of measurement $\mathbf{X}$. If we further assume that $\bar{g}(\Theta_0) = \Theta_0$, $\bar{g}(\Theta_1) = \Theta_1$, then the model and the decision problem are said to be invariant to the group $\mathcal{G}$. The orbits of $\mathbf{X}$ under actions of $\mathcal{G}$ are defined by

$$\mathbf{X} \equiv \mathbf{Y} \text{ if } \exists\, g \in \mathcal{G} \text{ such that } \mathbf{Y} = g(\mathbf{X}).$$

The orbits of $\theta$ under actions of $\bar{\mathcal{G}}$ are similarly defined. Note that to capture natural invariance of the model, the groups $\mathcal{G}$ and $\bar{\mathcal{G}}$ must have group actions with the largest possible degrees of freedom among all groups leaving the decision problem invariant.

The principle of invariance stipulates that any optimal decision rule should only depend on $\mathbf{X}$ through the maximal invariant $\mathbf{Z} = Z(\mathbf{X})$ which indexes the invariance orbits in the sense that

1. (invariant property) $Z(g(\mathbf{X})) = Z(\mathbf{X}), \forall g \in \mathcal{G}$
2. (maximal property) $Z(\mathbf{X}) = Z(\mathbf{Y}) \Rightarrow \mathbf{Y} = g(\mathbf{X}), g \in \mathcal{G}$.

Clearly, the maximal invariant is not unique. Any other functions of $\mathbf{X}$ related to $Z(\mathbf{X})$ in a one-to-one manner can be maximal invariant. It can also be shown that the probability density $f(\mathbf{Z}; \delta)$ of $\mathbf{Z}$ only depends on $\theta$ through a reduced set of parameters $\delta = \delta(\theta)$, which is the induced maximal invariant under $\bar{\mathcal{G}}$. Thus use of the reduced data $\mathbf{Z}$ gives us better chances of finding

a CFAR test whose false alarm rate is independent of $\theta$. In particular, when $\delta(\theta_0)$ is constant over $\theta_0 \in \Theta_0$, the distribution of $\mathbf{Z}$ under $H_0$ is fixed and therefore any test based on $\mathbf{Z}$ will automatically be CFAR.

### *B. Example: Unstructured Clutter Covariance*

We will first consider the case where the clutter is totally unknown. We use the image model in (4) and its partitioned form

$$\mathbf{X} = [\underline{x}_1 \ \mathbf{X}_2] = \begin{bmatrix} x_{11} & \underline{x}_{12} \\ \underline{x}_{21} & \mathbf{X}_{22} \end{bmatrix} \tag{6}$$

where $\underline{x}_1$ is the first subimage which may contain the target and all the target energy has been put into the first pixel $x_{11}$ of this subimage. This is the case studied by Kelly [9], and the results are briefly reviewed here to help illustrate the application of the GLR and invariance principles discussed previously. This will help the reader understand more complicated structured models of interest, covered later in this paper.

#### B.1 GLR Approach

The problem is to decide whether $a$ is 0 or not when $\mathbf{R}$ is unknown, and the pdf of $\mathbf{X}$ is

$$f(\mathbf{X}) = \frac{1}{\pi^{mn}|\mathbf{R}|^n} \exp\left[-tr\{\mathbf{R}^{-1}\mathbf{L}\}\right] \tag{7}$$

where $\mathbf{L} = (\underline{x}_1 - a\underline{\varepsilon}_1)(\underline{x}_1 - a\underline{\varepsilon}_1)^H + \sum_{i=2}^n \underline{x}_i \underline{x}_i^H$. We derive the GLR by maximizing the likelihood ratio over $a$ and $\mathbf{R}$, i.e. by replacing them with their MLEs:

$$l_1 = \frac{\max_{\theta\in\Theta_1} f(\mathbf{X};\theta)}{\max_{\theta\in\Theta_0} f(\mathbf{X};\theta)} = \frac{\max_a f(\mathbf{X}; a, \hat{\mathbf{R}}_1)}{f(\mathbf{X}; 0, \hat{\mathbf{R}}_0)}$$

where $\hat{\mathbf{R}}_0$ and $\hat{\mathbf{R}}_1$ are the sample covariance matrices under $H_0$ and $H_1$, respectively. To ensure these matrices be nonsingular with probability one, we must impose the condition that $n > m$. After some algebra, we obtain the following simple form of the GLR for this example by taking the $n$-th root of $l_1$:

$$\sqrt[n]{l_1} = \max_a \left\{ \frac{1 + \underline{x}_1^H (\mathbf{X}_2 \mathbf{X}_2^H)^{-1} \underline{x}_1}{1 + (\underline{x}_1 - a\underline{\varepsilon}_1)^H (\mathbf{X}_2 \mathbf{X}_2^H)^{-1} (\underline{x}_1 - a\underline{\varepsilon}_1)} \right\}. \tag{8}$$

It remains to maximize this ratio over the unknown complex amplitude $a$. This can be done by completing the square in the denominator of (8) and the GLR test is equivalent to $1 - 1/\sqrt[n]{l_1}$,

denoted $T_{Ku}$:

$$T_{Ku} = \frac{|\underline{\varepsilon}_1^T(\mathbf{X}_2\mathbf{X}_2^H)^{-1}\underline{x}_1|^2}{\underline{\varepsilon}_1^T(\mathbf{X}_2\mathbf{X}_2^H)^{-1}\underline{\varepsilon}_1 \cdot \{1+\underline{x}_1^H(\mathbf{X}_2\mathbf{X}_2^H)^{-1}\underline{x}_1\}}. \tag{9}$$

This test was obtained by Kelly [9] and will be called the unstructured Kelly's test.

### B.2 Invariance Approach

We define the following group of transformations acting on $\mathbf{X}$ as

$$g(\mathbf{X}) = \mathbf{FXH} = \begin{bmatrix} \beta_1 & \underline{\beta}_2^H \\ \underline{0} & \mathbf{M} \end{bmatrix} \mathbf{X} \begin{bmatrix} 1 & \underline{0}^T \\ \underline{0} & \mathbf{U} \end{bmatrix} \tag{10}$$

where $\beta_1 \neq 0$, $\underline{\beta}_2(1\times(m-1))$ and $\mathbf{M}((m-1)\times(m-1))$ are arbitrary, and $\mathbf{U}((n-1)\times(n-1))$ is a unitary matrix. Then with the model $\mathbf{X}$ in (4), we have $g(\mathbf{X}) = \tilde{a}\underline{\varepsilon}_1\underline{e}_1^T + \tilde{\mathbf{N}}$ where $\tilde{a} = \beta_1 a$ and $\tilde{\mathbf{N}}$ is still zero-mean Gaussian with $cov[vec(\tilde{\mathbf{N}})] = \mathbf{FRF}^H \bigotimes \mathbf{I}_n$. Thus the problem remains unchanged under this group since only the unknown $a$ and $\mathbf{R}$ are replaced by $\beta_1 a$ and $\mathbf{FRF}^H$, respectively. This group is also the group whose actions have the largest possible number of free parameters yet still ensuring that the decision problem and the model remain unchanged. Indeed if the full linear group of row actions were used, i.e. the first column of $\mathbf{F}$ in (10) were to be arbitrary, the signal spatial structure $\underline{\varepsilon}_1$ would not be preserved. Likewise, if a larger group of right-multiplying matrices than $\mathbf{H}$ in (10) were applied to the columns of $\mathbf{X}$, the independence of the columns of $\mathbf{X}$ or the temporal (chip) structure $\underline{e}_1$ of the signal would not be preserved.

Once the invariant group of transformations is obtained, we can now define a set of statistics, i.e. maximal invariants, which indexes the orbits of $\mathbf{X}$ under this group. With the model (6) and the group of transformations (10), it was shown in [7] that the maximal invariant is 2-dimensional:

$$\begin{aligned} z_{1'} &= \underline{x}_1^H(\mathbf{X}_2\mathbf{X}_2^H)^{-1}\underline{x}_1, \\ z_2 &= \underline{x}_{21}^H(\mathbf{X}_{22}\mathbf{X}_{22}^H)^{-1}\underline{x}_{21}. \end{aligned} \tag{11}$$

It is easily shown that that $\{z_{1'}, z_2\}$ is equivalent to $\{z_1, z_2\}$ where

$$z_1 = \frac{\left|x_{11} - \underline{x}_{12}\mathbf{X}_{22}^H(\mathbf{X}_{22}\mathbf{X}_{22}^H)^{-1}\underline{x}_{21}\right|^2}{\underline{x}_{12}\left[\mathbf{I} - \mathbf{X}_{22}^H(\mathbf{X}_{22}\mathbf{X}_{22}^H)^{-1}\mathbf{X}_{22}\right]\underline{x}_{12}^H}$$

since $z_{1'} = z_1 + z_2$ [16, Proposition 1]. The representation of $z_1$ gives it an interpretation as the estimated $\underline{s}$-prediction SNR, i.e. the ratio of the magnitude squared of the least-squares target estimation error to that of the least-squares clutter prediction error, where $\underline{x}_{12}\mathbf{X}_{22}^H(\mathbf{X}_{22}\mathbf{X}_{22}^H)^{-1}\underline{x}_{21}$

is the least-squares estimate of $x_{11}$ given $\underline{x}_{21}$ and $\mathbf{X}_2$. $z_1$ will be large when the clutter component can be accurately predicted and subtracted from the target cell, thereby enhancing the presence of the target. $z_2$ is the normalized sample correlation between primary and secondary data whose distribution is the same under $H_0$ and $H_1$. Thus it is an ancillary statistic [23].

Any invariant test will be functions of $z_1$ and $z_2$, and it is shown in [9] that the Kelly's test (9) is one of them:

$$T_{Ku} = \frac{z_1}{1 + z_1 + z_2} = \frac{z_1/(1+z_2)}{1 + z_1/(1+z_2)}. \tag{12}$$

$T_{Ku}$ is monotone increasing in $z_1/(1+z_2)$ and thus $z_2$ plays the role of a data-dependent normalization of the estimated $\underline{s}$-prediction SNR, $z_1$. This normalization has a distribution which is independent of the parameters and converges in distribution to a Chi-square random variable with $(m-1)$ degrees of freedom.

## IV. Application to a Target Straddling Clutter Boundary

Now we consider the problem of detecting a known target straddling the boundary of two independent clutter regions. From the model (5), the measurement matrix $\mathbf{X}$ can be partitioned as

$$\mathbf{X} = \begin{bmatrix} \underline{x}_{A1} & \mathbf{X}_{A2} \\ \underline{x}_{B1} & \mathbf{X}_{B2} \end{bmatrix} = \begin{bmatrix} x_{A11} & \underline{x}_{A12} \\ \underline{x}_{A21} & \mathbf{X}_{A22} \\ x_{B11} & \underline{x}_{B12} \\ \underline{x}_{B21} & \mathbf{X}_{B22} \end{bmatrix} \tag{13}$$

where $\underline{x}_{A1}$ and $\underline{x}_{B1}$ are the primary vectors which may contain the separated canonical parts of a known target, $\underline{s}_A$ and $\underline{s}_B$, respectively, with the unknown common amplitude $a$. Here we remove the tildes from $\tilde{\underline{s}}_A$ and $\tilde{\underline{s}}_B$ for notational convenience. Under $H_0$, any of the i.i.d. columns of $\mathbf{X}$ will be multivariate Gaussian with zero mean and a covariance matrix $\mathbf{R}$ having a block diagonal structure as defined in (1).

### A. GLR Tests

Let $\{\underline{x}_{Ai}\}_{i=1}^n$ and $\{\underline{x}_{Bi}\}_{i=1}^n$ represent the i.i.d. columns of the two uncorrelated matrices $\mathbf{X}_A$ and $\mathbf{X}_B$, respectively, then the pdf of $\mathbf{X}$ factors as $f(\mathbf{X}) = f(\mathbf{X}_A)f(\mathbf{X}_B)$ where $f(\mathbf{X}_A)$ and $f(\mathbf{X}_B)$ are defined similarly as (7) for each region. As in the unstructured case, the GLR maximization

can be performed for the unknown covariance matrices $\mathbf{R}_A$ and $\mathbf{R}_B$ by replacing them with their MLEs:

$$\Lambda = \max_a \frac{f(\mathbf{X}_A; a, \hat{\mathbf{R}}_{A1}) f(\mathbf{X}_B; a, \hat{\mathbf{R}}_{B1})}{f(\mathbf{X}_A; 0, \hat{\mathbf{R}}_{A0}) f(\mathbf{X}_B; 0, \hat{\mathbf{R}}_{B0})}.$$

Here, the required condition for non-singularity of the estimated covariance matrices ($n > m$) is relaxed since we need only $n > \max\{m_A, m_B\}$. GLR test statistics are listed in Table I for 3 structured cases where

$$\begin{aligned} p(a, \underline{s}_A, \mathbf{X}_A) &= (\underline{x}_{A1} - a\underline{s}_A)^H (\mathbf{X}_{A2}\mathbf{X}_{A2}^H)^{-1} (\underline{x}_{A1} - a\underline{s}_A) \\ q(a, \underline{s}_B, \mathbf{X}_B) &= \mathrm{tr}\left\{ (\mathbf{X}_B - a\underline{s}_B \underline{e}_1^T)^H (\mathbf{X}_B - a\underline{s}_B \underline{e}_1^T) \right\} \end{aligned}$$

and complete derivations can be found in [16]. Note that those GLRs still involve a maximization over the unknown amplitude $a$ in a complex quartic equation and cannot be represented in closed form. However, for real-valued data the roots of the quartic equation are explicit. For complex data we implement the GLR tests, derived under the structured cases, using numerical root finding and compare their performance in Section VI.

GLR 2 can be reduced to either of $l_1$ in (8) for $\mathbf{X}_A$ alone or the GLR over $\mathbf{X}_B$ alone which can be simplified to

$$l_2 = \max_a \left\{ \frac{q(0, \underline{s}_B, \mathbf{X}_B)}{q(a, \underline{s}_B, \mathbf{X}_B)} \right\}^{m_B n}.$$

We named it $l_2$ after the previous unstructured GLR test statistic $l_1$ in (8). As in $l_1$, the maximization in unstructured $l_2$ can be completed and we have the equivalent form of this GLR:

$$1 - \frac{1}{\sqrt[m_B n]{l_2}} = \frac{|x_{B11}|^2}{\sum_{i=1}^n |\underline{x}_{Bi}|^2}. \tag{14}$$

Similarly, we can also show that GLR 3 can be reduced to either of $l_1$ in (8) for $\mathbf{X}_A$ alone or the GLR $l_3$ for $\mathbf{X}_B$ alone which is equivalent to

$$\ln l_3 = |x_{B11}|^2. \tag{15}$$

### *B. MI Tests*

In this section we apply the invariance principle to the structured covariance cases studied above. For each case, MI test is proposed based on the maximal invariants and compared to the previous results of Kelly [9] and Bose and Steinhardt [7].

B.1 Case 1: $\mathbf{R}_A > 0, \mathbf{R}_B > 0$

In this case, we can construct a structured group of transformations on $\mathbf{X}$ which is extended from (10):

$$g(\mathbf{X}) = \begin{bmatrix} \begin{bmatrix} \beta & \underline{\beta}_A^H \\ \underline{0} & \mathbf{M}_A \end{bmatrix} & \mathbf{X}_A & \begin{bmatrix} 1 & \underline{0}^T \\ \underline{0} & \mathbf{U}_A \end{bmatrix} \\ \begin{bmatrix} \beta & \underline{\beta}_B^H \\ \underline{0} & \mathbf{M}_B \end{bmatrix} & \mathbf{X}_B & \begin{bmatrix} 1 & \underline{0}^T \\ \underline{0} & \mathbf{U}_B \end{bmatrix} \end{bmatrix} \tag{16}$$

where $\beta \neq 0$, $\underline{\beta}_A(1 \times (m_A - 1))$, $\underline{\beta}_B(1 \times (m_B - 1))$, $\mathbf{M}_A((m_A - 1) \times (m_A - 1))$ and $\mathbf{M}_B((m_B - 1) \times (m_B - 1))$ are arbitrary, and $\mathbf{U}_A$ and $\mathbf{U}_B$ are $((n-1) \times (n-1))$ unitary matrices. Showing the invariant property of this group is analogous to the unstructured example. With the model in (5) and the partition in (13), it was shown in [7] that the maximal invariant under (16) is 5-dimensional:

$$\begin{aligned} z_{A1} &= |u_A|^2 / D_A, \\ z_{A2} &= \underline{x}_{A21}^H (\mathbf{X}_{A22} \mathbf{X}_{A22}^H)^{-1} \underline{x}_{A21}, \\ z_{B1} &= |u_B|^2 / D_B, \\ z_{B2} &= \underline{x}_{B21}^H (\mathbf{X}_{B22} \mathbf{X}_{B22}^H)^{-1} \underline{x}_{B21}, \\ z_{AB} &= u_A / u_B \end{aligned} \tag{17}$$

where the subscripts denote whether the quantities are computed over the region A, B or both A and B, and

$$\begin{aligned} u_A &= x_{A11} - \underline{x}_{A12} \mathbf{X}_{A22}^H (\mathbf{X}_{A22} \mathbf{X}_{A22}^H)^{-1} \underline{x}_{A21}, \\ D_A &= \underline{x}_{A12} \left[ \mathbf{I} - \mathbf{X}_{A22}^H (\mathbf{X}_{A22} \mathbf{X}_{A22}^H)^{-1} \mathbf{X}_{A22} \right] \underline{x}_{A12}^H. \end{aligned}$$

$u_B$ and $D_B$ can be defined similarly over $\mathbf{X}_B$. It can be shown that $z_{AB}$ can be replaced by

$$z_{AB'} = \frac{|u_A/s_A - u_B/s_B|^2}{D_A/|s_A|^2 + D_B/|s_B|^2}$$

or

$$z_{AB''} = \frac{|u_A/s_A - u_B/s_B|^2}{q_A D_A/|s_A|^2 + q_B D_B/|s_B|^2} \tag{18}$$

where $q_A = 1 + z_{A1} + z_{A2}$ and $q_B = 1 + z_{B1} + z_{B2}$ [16, Proposition 2]. $z_{A1}$ and $z_{B1}$ correspond to the estimated $\underline{s}$-prediction SNRs in region A and B, respectively. $z_{A2}$ and $z_{B2}$ are the normalized

sample correlation between primary and secondary data pixels in region A and B, respectively. We can see that $z_{A1}$ and $z_{A2}$ correspond to $z_1$ and $z_2$ in the unstructured case (11) applied to region A, and $z_{B1}$ and $z_{B2}$ correspond to those applied to region B. The coupling term, $z_{AB}$, $z_{AB'}$, or $z_{AB''}$, not present in the unstructured test, captures the common amplitude $a$ for both regions.

A natural modification of Kelly's test (9) which reflects the block covariance structure was proposed by Kelly in [24] and later by Bose and Steinhardt [7]:

$$T_{Ks} = \frac{\left|\underline{s}^H \mathbf{K}^{-1} \underline{x}_1\right|^2}{\underline{s}^H \mathbf{K}^{-1} \underline{s} \cdot \{1 + \underline{x}_1^H \mathbf{K}^{-1} \underline{x}_1\}} \tag{19}$$

where $\underline{x}_1 = [\underline{x}_{A1}^H \ \underline{x}_{B1}^H]^H$, $\underline{s} = [\underline{s}_A^H \ \underline{s}_B^H]^H$ and

$$\mathbf{K} = \begin{bmatrix} \mathbf{X}_{A2}\mathbf{X}_{A2}^H & \mathbf{O} \\ \mathbf{O} & \mathbf{X}_{B2}\mathbf{X}_{B2}^H \end{bmatrix}.$$

The structured Kelly's test (19) can be equivalently expressed [16] in terms of the maximal invariants (17) as

$$T_{Ks} = \frac{z_{A1} + z_{B1} - z_{AB'}}{1 + z_{A1} + z_{A2} + z_{B1} + z_{B2}}. \tag{20}$$

Note that the denominator of $T_{Ks}$ essentially modulates the sum $z_{A1} + z_{B1}$ of $\underline{s}$-prediction SNRs by the sum of the associated ancillary statistics $z_{A2} + z_{B2}$. This has the effect of attenuating the individual $\underline{s}$-prediction SNRs in each region when both SNRs are strong.

Alternatively, by the maximal invariant representation of $T_{Ks}$, we can obtain another invariant test:

$$T_1 = \frac{\left| \begin{bmatrix} \underline{s}_A^H \underline{s}_B^H \end{bmatrix} \begin{bmatrix} q_A \mathbf{X}_{A2}\mathbf{X}_{A2}^H & \mathbf{O} \\ \mathbf{O} & q_B \mathbf{X}_{B2}\mathbf{X}_{B2}^H \end{bmatrix}^{-1} \begin{bmatrix} \underline{x}_{A1} \\ \underline{x}_{B1} \end{bmatrix} \right|^2}{\begin{bmatrix} \underline{s}_A^H \underline{s}_B^H \end{bmatrix} \begin{bmatrix} q_A \mathbf{X}_{A2}\mathbf{X}_{A2}^H & \mathbf{O} \\ \mathbf{O} & q_B \mathbf{X}_{B2}\mathbf{X}_{B2}^H \end{bmatrix}^{-1} \begin{bmatrix} \underline{s}_A \\ \underline{s}_B \end{bmatrix}}. \tag{21}$$

Note that $q_A$ and $q_B$ are placed in the estimated covariance matrix to separate the A and B coupled denominator in (20). This is equivalent to:

$$T_1 = \frac{z_{A1}}{1 + z_{A1} + z_{A2}} + \frac{z_{B1}}{1 + z_{B1} + z_{B2}} - z_{AB''} \tag{22}$$

where a different coupling term $z_{AB''}$ given in (18) is used instead of $z_{AB'}$ [16]. Unlike (20) the $\underline{s}$-prediction SNRs are normalized in an independent uncoupled manner. The MI test (22) will be shown to outperform (20) for some important situations.

### B.2 Case 2: $\mathbf{R}_A > 0, \mathbf{R}_B = \sigma^2\mathbf{I}$

Now suppose $\mathbf{R}_B = \sigma^2\mathbf{I}$ with unknown $\sigma^2$, then the appropriate invariant group of transformations in this case is

$$g(\mathbf{X}) = \left[ \begin{array}{cc} \left[ \begin{array}{cc} \beta & \underline{\beta}_A^H \\ \underline{0} & \mathbf{M}_A \end{array} \right] & \mathbf{X}_A \left[ \begin{array}{cc} 1 & \underline{0}^T \\ \underline{0} & \mathbf{U}_A \end{array} \right] \\ \beta & \mathbf{X}_B \left[ \begin{array}{cc} 1 & \underline{0}^T \\ \underline{0} & \mathbf{U}_B \end{array} \right] \end{array} \right] \tag{23}$$

since $\mathbf{X}_B$ still remains Gaussian under this group except that $a$ and $\sigma^2$ are replaced by $\tilde{a} = \beta a$ and $\tilde{\sigma}^2 = (\beta\sigma)^2$ [7]. Similarly to (16), the same scaling factor $\beta$ captures the common amplitude in both regions. With the partition in (13), the maximal invariant [7] under the group of transformations in (23) is composed of $z_{A1}$ and $z_{A2}$ in (17), and

$$\begin{aligned} z_B &= \frac{|x_{B11}|^2}{\sum_{i=1}^n |\underline{x}_{Bi}|^2}, \\ z_{AB} &= u_A / x_{B11}. \end{aligned} \tag{24}$$

We have equivalent forms [16, Proposition 3] for $z_B$ and $z_{AB}$: $z_B$ can be replaced by

$$z_{B'} = \frac{|x_{B11}|^2}{|\underline{x}_{B12}|^2 + |\underline{x}_{B21}|^2 + |\mathbf{X}_{B22}|_F^2}, \tag{25}$$

and $z_{AB}$ can be replaced by either of

$$z_{AB'} = \frac{|u_A/s_A - x_{B11}/s_B|^2}{\rho D_A/|s_A|^2 + v_1/|s_B|^2} \tag{26}$$

where

$$\begin{aligned} \rho &= \{(n - m_A)(1 + z_{A2})\}^{-1}, \\ v_1 &= \{|\underline{x}_{B12}|^2 + |\underline{x}_{B21}|^2 + |\mathbf{X}_{B22}|_F^2\}/(m_B n - 1), \end{aligned} \tag{27}$$

or

$$z_{AB''} = \frac{|u_A/s_A - x_{B11}/s_B|^2}{q_A D_A/|s_A|^2 + v_2/|s_B|^2} \tag{28}$$

where

$$\begin{aligned} q_A &= 1 + z_{A1} + z_{A2}, \\ v_2 &= \sum_{i=1}^{n} |\underline{x}_{Bi}|^2 / m_B. \end{aligned} \tag{29}$$

In (24) and (25) $z_B$ and $z_{B'}$ are the maximal invariants for the case that only region B is considered, and the coupling terms $z_{AB}, z_{AB''}$ are present due to the common scaling factor $\beta$ in regions A and B which preserves overall target amplitude $a$.

Bose and Steinhardt derived similar maximal invariants in the context of array detection problems in [7]. Based on these statistics they proposed an invariant test which was shown to be approximately CFAR and took the form:

$$T_{BS} = \frac{\left| \begin{bmatrix} \underline{s}_A^H & \underline{s}_B^H \end{bmatrix} \begin{bmatrix} \rho \mathbf{X}_{A2} \mathbf{X}_{A2}^H & \mathbf{O} \\ \mathbf{O} & v_1 \mathbf{I} \end{bmatrix}^{-1} \begin{bmatrix} \underline{x}_{A1} \\ \underline{x}_{B1} \end{bmatrix} \right|^2}{\begin{bmatrix} \underline{s}_A^H & \underline{s}_B^H \end{bmatrix} \begin{bmatrix} \rho \mathbf{X}_{A2} \mathbf{X}_{A2}^H & \mathbf{O} \\ \mathbf{O} & v_1 \mathbf{I} \end{bmatrix}^{-1} \begin{bmatrix} \underline{s}_A \\ \underline{s}_B \end{bmatrix}} \tag{30}$$

where $\rho$ and $v_1$ are as in (27). An equivalent form [16] for (30) is:

$$T_{BS} = (n - m_A) z_{A1} (1 + z_{A2}) + (m_B n - 1) z_{B'} - z_{AB'}. \tag{31}$$

By considering the structures of both the GLR 2 and the MI test 1 (21), we can construct another invariant test statistic $T_2$ which is same as (30) except that, as in (21), $\rho$ and $v_1$ in (30) are replaced by $q_A$ and $v_2$ defined in (29). The resultant test takes the form [16]

$$T_2 = \frac{z_{A1}}{1 + z_{A1} + z_{A2}} + m_B \cdot z_B - z_{AB''}. \tag{32}$$

Thus the weighting between the terms from regions A and B is maintained as in GLR 2, and this test reduces exactly to the unstructured tests: (12) for $\mathbf{X}_A$ alone or (14) for $\mathbf{X}_B$ alone. This reduction does not hold for Bose and Steinhardt's test (31).

### B.3 Case 3: $\mathbf{R}_A > 0, \mathbf{R}_B = \mathbf{I}$

For this case, the invariant group of transformations is defined as

$$g(\mathbf{X}) = \left[ \begin{array}{cc} \left[ \begin{array}{cc} \beta & \underline{\beta}_A^H \\ \underline{0} & \mathbf{M}_A \end{array} \right] & \mathbf{X}_A \left[ \begin{array}{cc} 1 & \underline{0}^T \\ \underline{0} & \mathbf{U}_A \end{array} \right] \\ & \mathbf{X}_B \left[ \begin{array}{cc} 1 & \underline{0}^T \\ \underline{0} & \mathbf{U}_B \end{array} \right] \end{array} \right]$$

where, unlike the previous two cases, there is no scaling term on the left of $\mathbf{X}_B$ since the variance is exactly known in $\mathbf{X}_B$ and must not be altered by the group actions. Thus the set of maximal invariants will not include any coupling term $z_{AB}$ from regions A and B.

An MI test can be constructed in much the same way as $T_2$ was constructed;

$$T_3 = \frac{z_{A1}}{q_A} + \frac{1}{n}|x_{B11}|^2 - \frac{|u_A/s_A - x_{B11}/s_B|^2}{q_A D_A/|s_A|^2 + n/|s_B|^2}. \tag{33}$$

This test is equivalent to $T_2$ when $v_2$ is replaced by $v_3 = n$. Note that $|x_{B11}|^2$ can be interpreted as the maximal invariant when only region B is considered. This test also reduces to either of the unstructured cases: (12) for $\mathbf{X}_A$ alone or (15) for $\mathbf{X}_B$ alone.

In Table II, MI tests are reproduced as functions of the maximal invariants under each case.

## V. Extension to One of $p$ Known Targets

Previously the target signature in the primary vector was assumed to be exactly known and the problem was to decide whether the one and only signal vector $\underline{s}$ is present or not. In real radar applications, however, a more realistic model must be considered. Suppose that we know the form of the target of interest, but do not know its position or orientation in the subimage chip. We assume that the target is totally contained in a chip, i.e. "coarse detection" has somehow been performed. An extension to the case where a target overlaps more than one chip can be handled in a similar manner to the within-chip positional uncertainty considered here, but is beyond the scope of this paper. Then different target signature vectors can be constructed accordingly. To accommodate this scenario, let the image model have an $m \times p$ matrix $\mathbf{S} = [\underline{s}_1, \ldots, \underline{s}_p]$ for $p$ target signatures:

$$a\,\mathbf{S}\,\underline{\epsilon}_k\,\underline{e}_1^T + \mathbf{N} \tag{34}$$

where $\underline{\epsilon}_k$ is a $p \times 1$ unit vector $[0, \ldots, 0, 1, 0, \ldots, 0]^T$ and '1' is in position $k$. Here $p \leq m$ for unstructured clutter or $p \leq \min\{m_A, m_B\}$ for structured clutter. The model (34) implies

that only one of the signatures, $\underline{s}_k$, may be present at a time in the primary vector, and in the structured case this signature vector is written as $\underline{s}_k = \left[\underline{s}_{Ak}^H \; \underline{s}_{Bk}^H\right]^H$.

For the GLR tests in Table I, it is easy to extend the results of the single target case to this multiple target case. We only need to replace $\underline{s}_A$ and $\underline{s}_B$ in the GLR tests with $\underline{s}_{Ak}$ and $\underline{s}_{Bk}$, and maximize over $k = 1, \ldots, p$, i.e.

$$\max_{k=1,\ldots,p} \frac{1}{n} \ln \Lambda(\underline{s}_{Ak}, \underline{s}_{Bk}).$$

Similarly, for the MI tests we also propose to maximize the test statistic over the $p$ target signatures. In the following, the invariance procedure is applied to (34) for both cases of unstructured and structured clutter. Due to length constraints, only the structured case of $\mathbf{R}_A > 0, \mathbf{R}_B > 0$ (Case 1) is treated in this paper.

### *A. Unstructured Case*

Since the set of possible signatures $\mathbf{S}$ is known, we can define the canonical model by left-multiplying (34) with the $m \times m$ matrix

$$\begin{bmatrix} (\mathbf{S}^H\mathbf{S})^{-1}\mathbf{S}^H \\ \mathbf{P}_S \end{bmatrix}$$

where the $(m-p) \times m$ matrix $\mathbf{P}_S$ is an orthogonal matrix to $(\mathbf{S}^H\mathbf{S})^{-1}\mathbf{S}^H$. Then we have the equivalent model

$$\mathbf{X} = a \begin{bmatrix} \underline{\epsilon}_k \\ \underline{0} \end{bmatrix} \underline{e}_1^T + \tilde{\mathbf{N}} \tag{35}$$

with $\tilde{\mathbf{N}}$ also zero-mean Gaussian with i.i.d. columns. This model (35) can be partitioned as in (3) where the $p \times 1$ vector $\underline{x}_{11}$ may contain any one of the target signatures which have been transformed to unit vectors $\{\underline{\epsilon}_k\}_{k=1}^p$. With this model, a group of transformations which preserves the decision problem is defined as

$$g(\mathbf{X}) = \begin{bmatrix} \Delta & \mathbf{B} \\ \mathbf{O} & \mathbf{M} \end{bmatrix} \mathbf{X} \begin{bmatrix} 1 & \underline{0}^T \\ \underline{0} & \mathbf{U} \end{bmatrix} \tag{36}$$

where $\Delta$ is a $p \times p$ diagonal matrix, $\mathbf{B}$ $(p \times (m-p))$ and $\mathbf{M}$ $((m-p) \times (m-p))$ are arbitrary, and $\mathbf{U}$ is an $(n-1) \times (n-1)$ unitary matrix. Note that by putting the model (34) into the canonical form (35), we must restrict $\Delta$ to a diagonal matrix in (36) instead of an arbitrary matrix in

order to preserve the model (35). This group of transformations with larger degrees of freedom will thus lead to a larger set of maximal invariants. The maximal invariant of the model (35) under the group of transformations in (36) is derived in [16, Proposition 4] and consists of $p+2$ functions of the measurement:

$$\begin{aligned} z_1 &= \underline{u}^H \mathbf{D}^{-1} \underline{u}, \\ z_2 &= \underline{x}_{21}^H (\mathbf{X}_{22}\mathbf{X}_{22}^H)^{-1} \underline{x}_{21}, \\ z_{3k} &= \underline{u}^H \mathbf{D}^{-1} \underline{\epsilon}_k (\underline{\epsilon}_k^T \mathbf{D}^{-1} \underline{\epsilon}_k)^{-1} \underline{\epsilon}_k^T \mathbf{D}^{-1} \underline{u} \end{aligned}$$

where $k = 1, \ldots, p$ and

$$\begin{aligned} \underline{u} &= \underline{x}_{11} - \mathbf{X}_{12}\mathbf{X}_{22}^H (\mathbf{X}_{22}\mathbf{X}_{22}^H)^{-1} \underline{x}_{21}, \\ \mathbf{D} &= \mathbf{X}_{12} \left[ \mathbf{I} - \mathbf{X}_{22}^H (\mathbf{X}_{22}\mathbf{X}_{22}^H)^{-1} \mathbf{X}_{22} \right] \mathbf{X}_{12}^H. \end{aligned} \tag{37}$$

The unstructured Kelly's test (9) can be modified by maximizing the likelihood ratio over $\{\underline{\epsilon}_k\}_{k=1}^p$ which reduces it to

$$T_{Ku} = \max_{k=1,\ldots,p} \frac{z_{3k}}{1 + z_1 + z_2}.$$

*B. Structured Clutter Covariance*

Next consider Case 1 ($\mathbf{R}_A > 0, \mathbf{R}_B > 0$) for the structured clutter covariance model. Then, similarly to the above unstructured model (35), the canonical image model can be defined as

$$\mathbf{X} = a \begin{bmatrix} \underline{\epsilon}_k \\ \underline{0}_A \\ \underline{\epsilon}_k \\ \underline{0}_B \end{bmatrix} \underline{e}_1^T + \mathbf{N} \tag{38}$$

where $\underline{0}_A$ and $\underline{0}_B$ are $(m_A - p) \times 1$ and $(m_B - p) \times 1$ zero vectors, respectively. Thus, this canonical form can be partitioned as (3) for each of $\mathbf{X}_A$ and $\mathbf{X}_B$, and the appropriate invariant group of transformations on $\mathbf{X}$ is

$$g(\mathbf{X}) = \begin{bmatrix} \begin{bmatrix} \Delta & \mathbf{B}_A \\ \mathbf{O} & \mathbf{M}_A \end{bmatrix} & \mathbf{X}_A & \begin{bmatrix} 1 & \underline{0}^T \\ \underline{0} & \mathbf{U}_A \end{bmatrix} \\ \begin{bmatrix} \Delta & \mathbf{B}_B \\ \mathbf{O} & \mathbf{M}_B \end{bmatrix} & \mathbf{X}_B & \begin{bmatrix} 1 & \underline{0}^T \\ \underline{0} & \mathbf{U}_B \end{bmatrix} \end{bmatrix} \tag{39}$$

where we have the same $p \times p$ diagonal matrix $\Delta$ for $\mathbf{X}_A$ and $\mathbf{X}_B$ to preserve the signal vector $\underline{\epsilon}_k$ and the same amplitude in both regions. With the model (38) and the group of transformations in (39), the maximal invariant is obtained in [16, Proposition 5] as

$$\begin{aligned}
z_{A1} &= \underline{u}_A^H \mathbf{D}_A^{-1} \underline{u}_A, \\
z_{A2} &= \underline{x}_{A21}^H (\mathbf{X}_{A22} \mathbf{X}_{A22}^H)^{-1} \underline{x}_{A21}, \\
z_{A3k} &= \underline{u}_A^H \mathbf{D}_A^{-1} \underline{\epsilon}_k (\underline{\epsilon}_k^T \mathbf{D}_A^{-1} \underline{\epsilon}_k)^{-1} \underline{\epsilon}_k^T \mathbf{D}_A^{-1} \underline{u}_A, \\
z_{B1} &= \underline{u}_B^H \mathbf{D}_B^{-1} \underline{u}_B, \\
z_{B2} &= \underline{x}_{B21}^H (\mathbf{X}_{B22} \mathbf{X}_{B22}^H)^{-1} \underline{x}_{B21}, \\
z_{B3k} &= \underline{u}_B^H \mathbf{D}_B^{-1} \underline{\epsilon}_k (\underline{\epsilon}_k^T \mathbf{D}_B^{-1} \underline{\epsilon}_k)^{-1} \underline{\epsilon}_k^T \mathbf{D}_B^{-1} \underline{u}_B, \\
z_{ABk} &= \frac{(\underline{\epsilon}_k^T \mathbf{D}_A^{-1} \underline{\epsilon}_k)^{-1} \underline{\epsilon}_k^T \mathbf{D}_A^{-1} \underline{u}_A}{(\underline{\epsilon}_k^T \mathbf{D}_B^{-1} \underline{\epsilon}_k)^{-1} \underline{\epsilon}_k^T \mathbf{D}_B^{-1} \underline{u}_B}
\end{aligned} \tag{40}$$

where $k = 1, \ldots, p$, and $\underline{u}_A$, $\underline{u}_B$, $\mathbf{D}_A$ and $\mathbf{D}_B$ can be defined as $\underline{u}$ and $\mathbf{D}$ in (37) over $\mathbf{X}_A$ alone or $\mathbf{X}_B$ alone. And $z_{ABk}$ can be replaced by

$$z_{ABk'} = \frac{\left| (\underline{\epsilon}_k^T \mathbf{D}_A^{-1} \underline{\epsilon}_k)^{-1} \underline{\epsilon}_k^T \mathbf{D}_A^{-1} \underline{u}_A - (\underline{\epsilon}_k^T \mathbf{D}_B^{-1} \underline{\epsilon}_k)^{-1} \underline{\epsilon}_k^T \mathbf{D}_B^{-1} \underline{u}_B \right|^2}{(\underline{\epsilon}_k^T \mathbf{D}_A^{-1} \underline{\epsilon}_k)^{-1} + (\underline{\epsilon}_k^T \mathbf{D}_B^{-1} \underline{\epsilon}_k)^{-1}} \tag{41}$$

or $z_{ABk''}$ which is equivalent to $z_{ABk'}$ except that $q_A \mathbf{D}_A$ and $q_B \mathbf{D}_B$ are substituted for $\mathbf{D}_A$ and $\mathbf{D}_B$, respectively, where again $q_A = 1 + z_{A1} + z_{A2}$ and $q_B = 1 + z_{B1} + z_{B2}$. Note that $z_{A1}$, $z_{A2}$, $z_{B1}$ and $z_{B2}$ are again equivalent to those in (17) except for the increased dimension ($p$ vs. 1) of these matrices.

We now generalize the structured Kelly's test, $T_{Ks}$ (19), and the MI test, $T_1$ (21), to $p > 1$. First, consider $T_{Ks}$ modified to fit the multiple signature model as a function of maximal invariants (40) and (41)

$$T_{Ks} = \max_{k=1,\ldots,p} \frac{z_{A3k} + z_{B3k} - z_{ABk'}}{1 + z_{A1} + z_{A2} + z_{B1} + z_{B2}}.$$

The MI test can also be modified similarly

$$T_1 = \max_{k=1,\ldots,p} \left\{ \frac{z_{A3k}}{1 + z_{A1} + z_{A2}} + \frac{z_{B3k}}{1 + z_{B1} + z_{B2}} - z_{ABk''} \right\}.$$

## VI. Numerical Results

To analyze the performance of the GLR and MI tests derived under the three structured clutter covariance assumptions (Case 1: $\mathbf{R}_A > 0, \mathbf{R}_B > 0$, Case 2: $\mathbf{R}_A > 0, \mathbf{R}_B = \sigma^2 \mathbf{I}$, and Case 3:

$\mathbf{R}_A > 0, \mathbf{R}_B = \mathbf{I}$), receiver operating characteristic (ROC) curves are generated and compared in this section. More examples are presented in [22]. In each simulation, we generated $n$ $10 \times 10$ subimages containing 2 independent clutter regions of area $m_A$ and $m_B$ pixels, respectively, and a $5 \times 5$ synthetic canonical target is inserted into the first subimage in such a manner to straddle the boundary of the two different regions. Each of the subimages is then concatenated into a column vector of size 100 to obtain a $100 \times n$ measurement matrix. Each of the ROC curves (probability of detection ($P_D$) vs. probability of false alarm ($P_{FA}$)) shown below was obtained after 500 simulations. We show results of experiments on a real synthetic-aperture radar (SAR) image where both of our GLR and MI tests were applied to a SAR clutter image with an inserted real target at various pose angles.

### *A. Comparison of ROC curves*

First, in Figs. 1 and 2, Cases 1 and 2 are considered separately under different assumptions on clutter covariance. The results for Case 3 are omitted since a large number of pixels ($m_B \times n$) are available to generate a good MLE of the unknown variance in region B and we were able to observe that the ROC curve for GLR 2 approaches that of the matched GLR 3. In each case, the three GLR tests in Table I and the three MI tests in Table II matched to one of the three cases are compared. Also shown are ROC curves for the following tests proposed by other authors: Kelly's structured test (20) matched to Case 1, and Bose and Steinhardt's invariant test (31) matched to Case 2. Those ROC curves are compared for different ratios of $m_A/m_B$ by up and down shifting the $10 \times 10$ windows used to collect the subimages along the boundary. In Fig. 1 for Case 1, the structured Kelly's test is as accurate as or better than the GLR and MI tests only for the smaller size covariance of (a). Also Bose and Steinhardt's test is more sensitive to $m_A$ and $m_B$ than MI test 2 and GLR 2, and its ROC falls below even those of the mismatched tests shown in Fig. 2 (b). This confirms the results from Section IV. For Case 1, we were able to achieve performance improvement by separating the same coupled denominator for both regions found in the matched Kelly's test (20). For Case 2, the ROC improvement over the matched Bose and Steinhardt's test is explained by the weighting between two different regions which is carefully managed in GLR 2 and MI test 2. Note that, however, neither the GLR nor the MI test uniformly outperforms the other. Of particular interest are the curve crossings in the low $P_{FA}$ regions between the GLR and the MI tests as in Fig. 1 (b).

The relative advantages of MI vs. GLR tests are more closely investigated in the next two

figures. In Figs. 3 and 4, we consider Cases 1 and 2, respectively. In (a) of both figures, we increased the number of chips $n$ while fixing SNR. Note that the GLR and MI tests have ROCs which are virtually indistinguishable for large $n$. In (b), however, we fixed $n$ and increased SNR. The $P_{FA}$ positions of the crossings of the ROCs for the GLR and MI tests decreased with increasing SNR. In particular, if one fixes a level of false alarm, say $P_{FA} = 0.1$, then note from Fig. 3 (b) that the GLR test dominates the MI test for SNR = 19 dB while the reverse is true for SNR = 7 dB. This behavior is best explained by the fact that at high SNR, the MLE is an accurate estimate of target amplitude, while at low SNR the MLE degrades significantly. Therefore, the GLR which depends on the accuracy of the MLE for accurate detection breaks down for low SNR.

Since both the structured GLR and MI tests can only be implemented with the known boundary separating two different regions, sensitivity of the tests to boundary estimation errors is illustrated in Fig. 5. In both cases, ROC curves obtained with the biased boundary are compared with those using the true boundary. As can be seen, the overall performance of each test is degraded with false information, but the relative advantages of the GLR and MI tests still can be observed.

### *B. Application to a Real Image*

Next, we consider an application to actual acquired complex-valued SAR imagery. In Fig. 6 the magnitude-only SAR image is shown. This corresponds to a rural scene near Redstone Arsenal at Huntsville, Alabama, reproduced from the data collected using the Sandia National Laboratories Twin Otter SAR sensor payload operating at X band (center frequency = 9.6 GHz, band width = 590 MHz). This clutter image consists of a forest canopy on top and a field on bottom, separated by a coarse boundary. The boundary was hand-extracted, and a sequence of $9 \times 7$ SLICY targets at different poses were also hand-extracted from the image data in Fig. 7. The images in Fig. 7 correspond to the same target but viewed at different pose angles of azimuth. The elevation of 39° was fixed for all poses. These images display the magnitudes of complex-valued SAR data which have been converted into decibels (dB). The data from which these images are reproduced was downloaded from the MSTAR SAR database at the Center for Imaging Science (www.cis.jhu.edu).

In a first experiment the target signature at pose of azimuth 163° from Fig. 7 (e) was tested at different positions along the boundary. In Fig. 6, the target is inserted additively with the

center at column 305 so that it straddles the boundary. From the realigned image in Fig. 8, we took subimages (chips) along the boundary by centering a $20 \times 20$ window at the boundary and sliding it over the image from left to right. Each of these subimages is then concatenated into a column vector of size $m = 400$ where $m_A = 200$ and $m_B = 200$. Since we need at least 200 secondary chips to implement the structured detectors, clutter-alone pixels above and below those $20 \times 20$ subimages taken along the boundary were used to generate enough secondary data for region A and B, respectively. Each of the subimages along the boundary was tested as a primary chip, and the test statistics derived under Case 1 were calculated and maximized over each possible location in the subimage. After normalizing the known target signature, we obtained the minimum magnitude of target amplitude required for each test to detect the target at the correct location. The resulting amplitude is the minimum detectable threshold for each of the detectors and these thresholds are shown in Table III for different number of secondary chips $(n-1)$. As can be seen, with a large number of chips $(n-1=250)$, both the GLR and MI tests perform as well as the structured Kelly's test. On the other hand, with a limited number of chips $(n-1=200)$, MI test 1 successfully detects the target down to a significantly lower threshold than for GLR 1 and structured Kelly detectors.

Next we maximized the test statistics over the different target poses in Fig. 7 as well as over all possible locations along the boundary. Again the normalized signature from Fig. 7 (e) was inserted with $|a| = 0.015$, and 250 secondary chips were obtained from the surrounding clutter. Test values for the 3 detectors under Case 1 are obtained using 9 different target signatures. For each test the peak values for 9 target signatures are plotted in Fig. 9. Note that all the tests successfully picked the signature at the true pose and location for this target amplitude.

As a final experiment minimum detectable amplitudes for the GLR and MI tests are obtained with a boundary extraction procedure utilizing Sobel's edge detection method [25]. Note that we only applied the estimation algorithm to the clutter-alone chips so as to evaluate the effect of boundary estimates on clutter covariance estimates. Table IV shows the results for 200 secondary chips using two different boundary extractions. As in the ROC simulation (Fig. 5), both detectors require larger target amplitudes for correct detection, but we conclude that the MI test remains more robust than the GLR test even in the presence of segmentation errors. In this experiment, the boundary between two regions was extracted using the simple Sobel operator. More sophisticated model-based methods of an automatic image segmentation, e.g. methods

such as proposed in [26], [27], [28], would potentially perform better than the Sobel operator.

## VII. Conclusion

The deep-hide scenario considered in this paper complicates the design of optimal target detectors. Both GLR and MI tests can be derived under block diagonal constraints imposed by the clutter covariance structure. Numerical results indicate that neither GLR nor MI tests dominate the other in terms of ROC performance. Both detectors have comparable performance when high estimator accuracy is attainable, e.g. for a large number of independent clutter samples, but otherwise the MI test is better especially in low $P_{FA}$. This property is also shown to be robust to segmentation errors. The results in this paper are generalizable to other applications where structured covariance information is available.

## References

[1] T. S. Ferguson, *Mathematical Statistics: A Decision Theoretic Approach*, New York: Academic Press, 1967.

[2] R. J. Muirhead, *Aspects of Multivariate Statistical Theory*, New York: Wiley, 1982.

[3] M. L. Eaton, *Group Invariance Applications in Statistics*, *Regional Conf. Series in Probability and Statistics*, vol. 1, Institute of Mathematical Statistics, 1989.

[4] L. L. Scharf, *Statistical Signal Processing: Detection, Estimation, and Time Series Analysis*, Reading, MA: Addison-Wesley, 1991.

[5] L. L. Scharf and D. W. Lytle, "Signal detection in Gaussian noise of unknown level: an invariance application," *IEEE Trans. Information Theory*, vol. IT-17, no. 4, pp. 404-411, Jul. 1971.

[6] S. Kraut and L. L. Scharf, "The CFAR adaptive subspace detector is a scale-invariant GLRT," *IEEE Trans. Signal Processing*, vol. 47, no. 9, pp. 2538-2541, Sep. 1999.

[7] S. Bose and A. O. Steinhardt, "A maximal invariant framework for adaptive detection with structured and unstructured covariance matrices," *IEEE Trans. Signal Processing*, vol. 43, no. 9, pp. 2164-2175, Sep. 1995.

[8] I. S. Reed, J. D. Mallet, and L. E. Brennan, "Rapid convergence rate in adaptive arrays," *IEEE Trans. Aerosp. Electron. Syst.*, vol. AES-10, no. 6, pp. 853-863, Nov. 1974.

[9] E. J. Kelly, "An adaptive detection algorithm," *IEEE Trans. Aerosp. Electron. Syst.*, vol. AES-22, pp. 115-127, Mar. 1986.

[10] F. C. Robey, D. R. Fuhrmann, E. J. Kelly, and R. Nitzberg, "A CFAR adaptive matched filter detector," *IEEE Trans. Aerosp. Electron. Syst.*, vol. AES-28, no. 1, pp. 208-216, Jan. 1992.

[11] S. G. Ricks and A. L. Swindlehurst, "Detection performance degradation due to miscalibrated arrays in airborne radar," *in Proc. IEEE Asilomar Conf. Signals, Systems, Computers*, Pacific Grove, CA, Nov. 1998, vol. 2, pp. 1532-1536.

[12] O. Macchi and B. C. Picinbono, "Estimation and detection of weak optical signals," *IEEE Trans. Information Theory*, vol. IT-18, no. 5, pp. 562-573, Sep. 1972.

[13] J. Y. Chen and I. S. Reed, "A detection algorithm for optical targets in clutter," *IEEE Trans. Aerosp. Electron. Syst.*, vol. AES-23, no. 1, pp. 46-59, Jan. 1987.

[14] D. Fuhrmann, "Application of Toeplitz covariance estimation to adaptive beamforming and detection," *IEEE Trans. Acoust., Speech, Signal Processing*, vol. 39, no. 10, pp. 2194-2198, Oct. 1991.

[15] A. O. Hero and C. Guillouet, "Robust detection of SAR/IR targets via invariance," *in Proc. IEEE Intl. Conf. Image Processing*, Santa Barbara, CA, Oct. 1997, vol. 3, pp. 472-475.

[16] H. S. Kim and A. O. Hero, "Comparison of GLR and invariance methods applied to adaptive target detection in structured clutter," Tech. Rep. 323, Communications and Signal Processing Lab., University of Michigan, Ann Arbor, MI, Nov. 2000 (http://www.eecs.umich.edu/systems/TechReportList.html).

[17] R. De Roo, F. Ulaby, A. El-Rouby, and A. Nashashibi, "MMW radar scattering statistics of terrain at near grazing incidence," *IEEE Trans. Aerosp. Electron. Syst.*, vol. 35, no. 3, pp. 1010-1018, Jul. 1999.

[18] E. J. Kelly and K. M. Forsythe, "Adaptive detection and parameter estimation for multidimensional signal models," Tech. Rep. 848, Lincoln Lab., Massachusetts Institute of Technology, Apr. 1989.

[19] I. A. Ibragimov and R. Z. Hasminskii, *Statistical Estimation: Asymptotic Theory*, New York: Springer-Verlag, 1981.

[20] H. L. Van Trees, *Detection, Estimation, and Modulation Theory: Part I*, New York: Wiley, 1968.

[21] E. L. Lehmann, *Testing Statistical Hypotheses*, New York: Wiley, 1959.

[22] H. S. Kim, "Adaptive target detection in radar imaging," Tech. Rep. 324, Communications and Signal Processing Lab., University of Michigan, Ann Arbor, MI, Apr. 2001.

[23] T. Kariya and B. K. Sinha, *Robustness of Statistical Tests*, San Diego: Academic Press, 1989.

[24] E. J. Kelly, "Adaptive detection in non-stationary interference," Tech. Rep. 724, Lincoln Lab., Massachusetts Institute of Technology, Jun. 1985.

[25] A. K. Jain, *Fundamentals of Digital Image Processing*, Englewood Cliffs, NJ: Prentice Hall, 1989.

[26] P. C. Smits and S. G. Dellepiane, "Synthetic aperture radar image segmentation by a detail preserving Markov random field approach," *IEEE Trans. Geosci. Remote Sensing*, vol. 35, no. 4, pp. 844-857, Jul. 1997.

[27] J. Dias, T. Silva, and J. Leitão, "Adaptive restoration of speckled SAR images using a compound random Markov field," *in Proc. IEEE Intl. Conf. Image Processing*, Chicago, IL, Oct. 1998, vol. 2, pp. 79-83.

[28] I. Pollak, A. S. Willsky, and H. Krim, "Image segmentation and edge enhancement with stabilized inverse diffusion equations," *IEEE Trans. Image Processing*, vol. 9, no. 2, pp. 256-266, Feb. 2000.

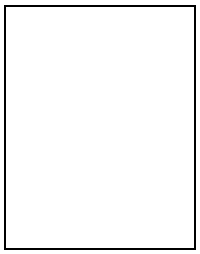

**Hyung Soo Kim** received the B.S. degree from Yonsei University, Seoul, Korea in 1994, and the Ph.D. degree from the University of Michigan, Ann Arbor in 2001, both in electrical engineering. His research interests include statistical signal and image processing, detection, estimation, and signal processing for communications.

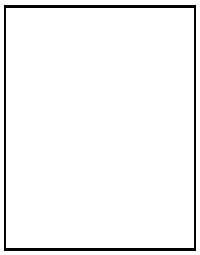

**Alfred O. Hero, III** was born in Boston, MA, in 1955. He received the B.S. degree (summa cum laude) from Boston University (1980) and the Ph.D degree from Princeton University (1984), both in electrical engineering. While at Princeton he held the G.V.N. Lothrop Fellowship in Engineering. Since 1984 he has been a Professor with the University of Michigan, Ann Arbor, where he has appointments in the Department of Electrical Engineering and Computer Science, the Department of Biomedical Engineering and the Department of Statistics. He has held visiting positions at I3S at the University of Nice, Sophia-Antipolis, France (2001), Ecole Normale Supérieure de Lyon (1999), Ecole Nationale Supérieure des Télécommunications, Paris (1999), Scientific Research Labs of the Ford Motor Company, Dearborn, Michigan (1993), Ecole Nationale des Techniques Avancees (ENSTA), Ecole Superieure d'Electricite, Paris (1990), and M.I.T. Lincoln Laboratory (1987 - 1989). His research has been supported by NIH, NSF, AFOSR, NSA, ARO, ONR and by private industry in the area of estimation and detection, statistical communications, signal processing and image processing.

He has served as Associate Editor for the IEEE Transactions on Information Theory. He was Chairman of the Statistical Signal and Array Processing (SSAP) Technical Committee and Treasurer of the Conference Board of the IEEE Signal Processing Society. He was Chairman for Publicity for the 1986 IEEE International Symposium on Information Theory (Ann Arbor, MI) and General Chairman of the 1995 IEEE International Conference on Acoustics, Speech, and Signal Processing (Detroit, MI). He was co-chair of the 1999 IEEE Information Theory Workshop on Detection, Estimation, Classification and Filtering (Santa Fe, NM) and the 1999 IEEE Workshop on Higher Order Statistics (Caesaria, Israel). He is currently a member of the Signal Processing Theory and Methods (SPTM) Technical Committee and Vice President (Finance) of the IEEE Signal Processing Society. He is Chair of Commission C (Signals and Systems) of the US National Commission of the International Union of Radio Science (URSI). Alfred Hero is a Fellow of the Institute of Electrical and Electronics Engineers (IEEE), a member of Tau Beta Pi, the American Statistical Association (ASA), the Society for Industrial and Applied Mathematics (SIAM), and the US National Commission (Commission C) of the International Union of Radio Science (URSI). He has received the 1998 IEEE Signal Processing Society Meritorious Service Award, the 1998 IEEE Signal Processing Society Best Paper Award, and the IEEE Third Millennium Medal.

| Case | $\mathbf{R}_A$ | $\mathbf{R}_B$ | Log GLR : $\frac{1}{n}\ln\Lambda = \max_a\{\cdot\}$ |
|---|---|---|---|
| 1 | ? | ? | $\ln\left[\frac{1+p(0,\underline{s}_A,\mathbf{X}_A)}{1+p(a,\underline{s}_A,\mathbf{X}_A)}\right] + \ln\left[\frac{1+p(0,\underline{s}_B,\mathbf{X}_B)}{1+p(a,\underline{s}_B,\mathbf{X}_B)}\right]$ |
| 2 | ? | $\sigma^2\mathbf{I}$ | $\ln\left[\frac{1+p(0,\underline{s}_A,\mathbf{X}_A)}{1+p(a,\underline{s}_A,\mathbf{X}_A)}\right] + m_B\cdot\ln\left[\frac{q(0,\underline{s}_B,\mathbf{X}_B)}{q(a,\underline{s}_B,\mathbf{X}_B)}\right]$ |
| 3 | ? | $\mathbf{I}$ | $\ln\left[\frac{1+p(0,\underline{s}_A,\mathbf{X}_A)}{1+p(a,\underline{s}_A,\mathbf{X}_A)}\right] + \frac{1}{n}\left[q(0,\underline{s}_B,\mathbf{X}_B) - q(a,\underline{s}_B,\mathbf{X}_B)\right]$ |

TABLE I

GLR tests for Cases 1, 2 and 3 derived in this paper (The notation '?' denotes that the matrix $\mathbf{R}_A$ or $\mathbf{R}_B$ is completely unknown but positive definite symmetric.)

| Case | $\mathbf{R}_A$ | $\mathbf{R}_B$ | MI test | |
|---|---|---|---|---|
| 1 | ? | ? | $T_{Ks} = \frac{z_{A1}+z_{B1}-z_{AB'}}{q_A+q_B-1}$ (20) | Kelly [24] |
| | | | $T_1 = \frac{z_{A1}}{q_A}+\frac{z_{B1}}{q_B}-\frac{\lvert u_A/s_A-u_B/s_B\rvert^2}{q_AD_A/\lvert s_A\rvert^2+q_BD_B/\lvert s_B\rvert^2}$ (22) | MI test 1 |
| 2 | ? | $\sigma^2\mathbf{I}$ | $T_{BS} = \frac{z_{A1}}{\rho}+\frac{\lvert x_{B11}\rvert^2}{v_1}-\frac{\lvert u_A/s_A-x_{B11}/s_B\rvert^2}{\rho D_A/\lvert s_A\rvert^2+v_1/\lvert s_B\rvert^2}$ (31) | Bose-Steinhardt [7] |
| | | | $T_2 = \frac{z_{A1}}{q_A}+\frac{\lvert x_{B11}\rvert^2}{v_2}-\frac{\lvert u_A/s_A-x_{B11}/s_B\rvert^2}{q_AD_A/\lvert s_A\rvert^2+v_2/\lvert s_B\rvert^2}$ (32) | MI test 2 |
| 3 | ? | $\mathbf{I}$ | $T_3 = \frac{z_{A1}}{q_A}+\frac{\lvert x_{B11}\rvert^2}{v_3}-\frac{\lvert u_A/s_A-x_{B11}/s_B\rvert^2}{q_AD_A/\lvert s_A\rvert^2+v_3/\lvert s_B\rvert^2}$ (33) | MI test 3 |

TABLE II

Maximal invariant tests (The notation '?' denotes that the matrix $\mathbf{R}_A$ or $\mathbf{R}_B$ is completely unknown but positive definite symmetric.)

| Test | $\lvert a\rvert$ | |
|---|---|---|
| | $(n-1=250)$ | $(n-1=200)$ |
| Structured Kelly | $1.407\times10^{-2}$ | $1.049\times10^{-1}$ |
| MI test 1 | $1.454\times10^{-2}$ | $0.609\times10^{-1}$ |
| GLR 1 | $1.462\times10^{-2}$ | $1.042\times10^{-1}$ |

TABLE III

Minimum detectable amplitudes for detection of the target at the correct location.

| Test | $\lvert a\rvert \quad (n-1=200)$ | |
|---|---|---|
| | (1) | (2) |
| MI test 1 | $0.609 \times 10^{-1}$ | $2.327 \times 10^{-1}$ |
| GLR 1 | $1.042 \times 10^{-1}$ | $8.655 \times 10^{-1}$ |

TABLE IV

MINIMUM DETECTABLE AMPLITUDES WITH (1) THE HAND-EXTRACTED BOUNDARY AND (2) THE ESTIMATED BOUNDARY.

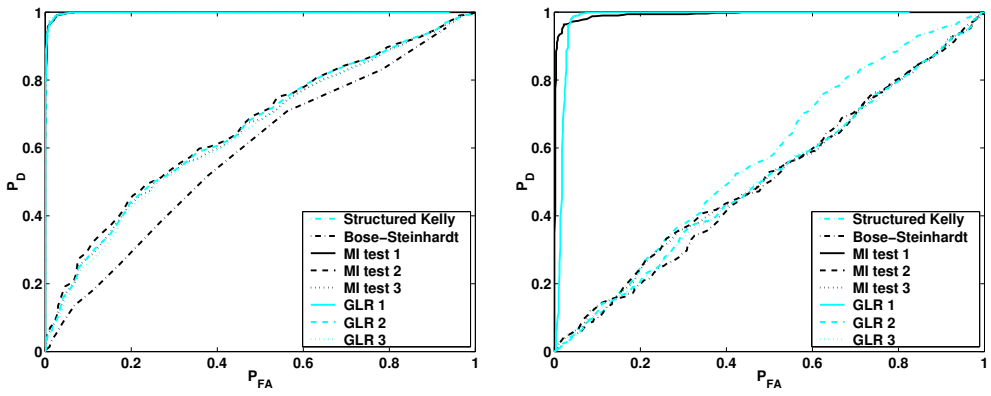


(a) $m_A = 50, m_B = 50$ (b) $m_A = 60, m_B = 40$

Fig. 1. ROC curves for Case 1 with different ratios of $m_A/m_B$ (SNR = 19 dB, $n = 61$).

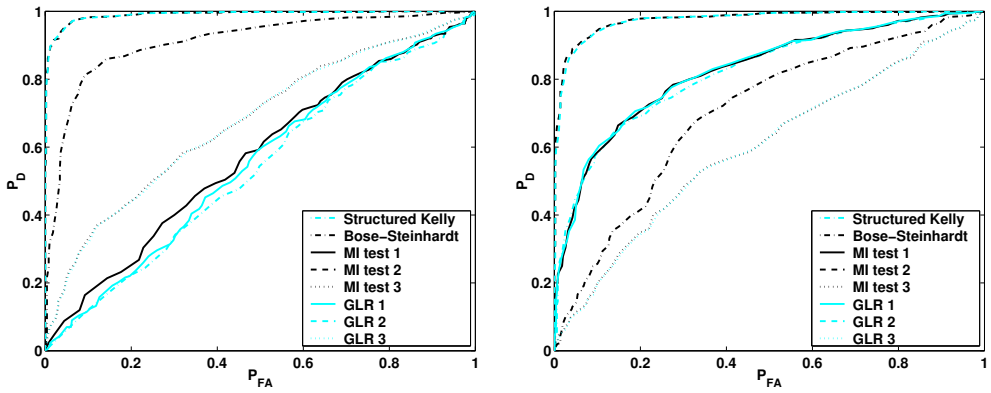


(a) $m_A = 40, m_B = 60$ (b) $m_A = 50, m_B = 50$

Fig. 2. ROC curves for Case 2 with different ratios of $m_A/m_B$ (SNR = 10 dB, $n = 61$).

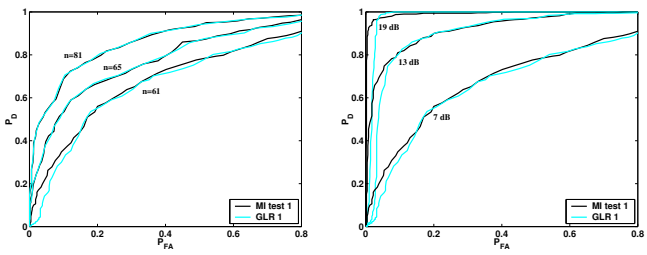


(a) SNR = 7 dB (b) $n = 61$

Fig. 3. Comparison of GLR and MI tests for Case 1 by (a) increasing $n$ with fixed SNR, and (b) increasing SNR with fixed $n$ ($m_A = 60, m_B = 40$).

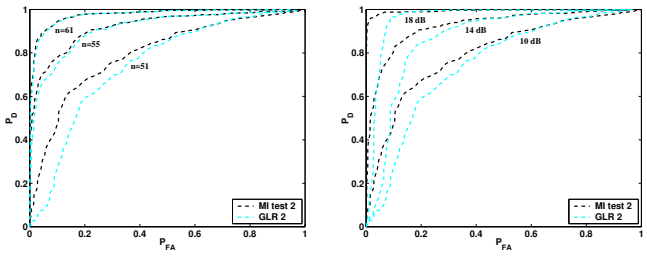


(a) SNR = 10 dB (b) $n = 51$

Fig. 4. Comparison of GLR and MI tests for Case 2 by (a) increasing $n$ with fixed SNR, and (b) increasing SNR with fixed $n$ ($m_A = 50, m_B = 50$).

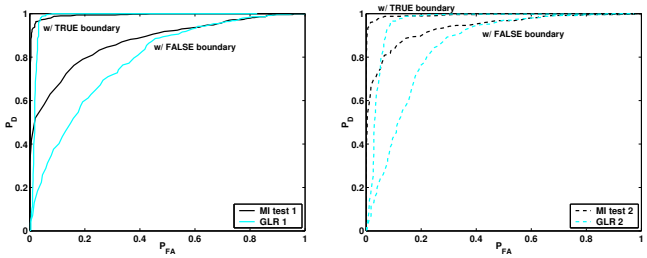


(a) Case 1 (b) Case 2

Fig. 5. Comparison of ROC curves using true boundaries and false boundaries (a) moved downward by one pixel, and (b) moved upward by one pixel in each snapshot (True values: (a) $m_A = 60, m_B = 40, n = 61$, (b) $m_A = 50, m_B = 50, n = 51$).

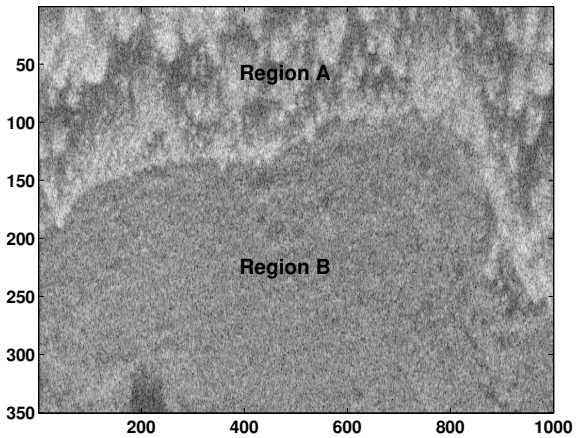


Fig. 6. Magnitude-only image of SAR clutter with target in Fig. 7 (e) straddling the boundary at column 305. Complex image was used in all simulations

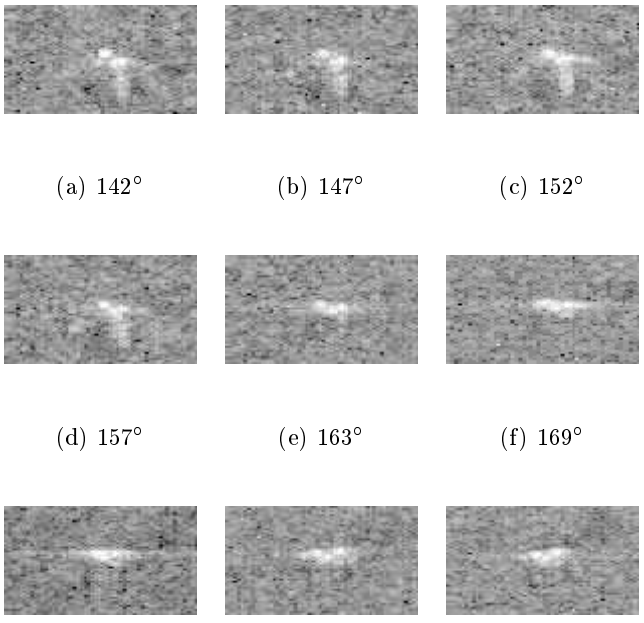

(a) 142° (b) 147° (c) 152°

(d) 157° (e) 163° (f) 169°

(g) 175° (h) 187° (i) 193°

Fig. 7. Magnitude images of SLICY canonical targets at elevation 39° and different azimuth angles. Image in (e) is inserted in Fig. 6.

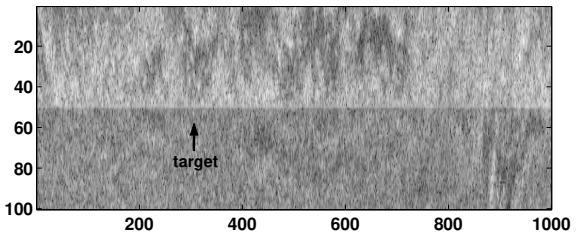


Fig. 8. Magnitude-only SAR image (Fig. 6) realigned along the extracted boundary. SLICY target is located at column 305 with $|a| = 0.015$. This target is just above the minimal detectable threshold for the three tests investigated in Fig. 9.

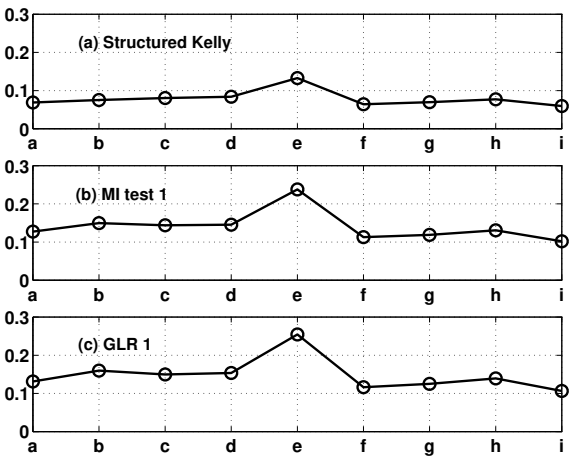


Fig. 9. Peak values obtained for 9 different target images in Fig. 7 ($|a| = 0.015, n - 1 = 250$).